

Cite this: *Dalton Trans.*, 2014, **43**, 2488

pH-controlled assembly of hybrid architectures based on Anderson-type polyoxometalates and silver coordination units†

Ying Hu,^a Haiyan An,^{*a} Xuan Liu,^a Jiqiu Yin,^{*b} Hui long Wang,^a Hua Zhang^a and Lin Wang^a

Three new architectures based on Anderson-type polyoxometalates, $(3\text{-H}_2\text{pya})[(3\text{-Hpya})_2\text{Ag}][\text{AgAlMo}_6\text{H}_6\text{O}_{24}] \cdot 3\text{H}_2\text{O}$ **1**, $\text{HNa}_2[(3\text{-pya})(3\text{-Hpya})\text{Ag}]_2[\text{AlMo}_6\text{H}_6\text{O}_{24}] \cdot 8\text{H}_2\text{O}$ **2** and $[(3\text{-Hpya})_2\text{Ag}][(\text{H}_2\text{O})_2\text{Ag}]_2[\text{AlMo}_6\text{H}_6\text{O}_{24}] \cdot 2\text{H}_2\text{O}$ **3** ($3\text{-Hpya} = 3\text{-}(3\text{-pyridyl)acrylic acid}$), have been synthesized at the different pH values and characterized by elemental analysis, IR spectroscopy, TG analysis, powder X-ray diffraction and single crystal X-ray diffraction. Compound **1** was obtained at lower pH value (2.50), and represents a 3D host-guest compound containing the Ag-3-Hpya coordination complex guest and the 3D $[\text{AgAlMo}_6\text{H}_6\text{O}_{24}]^{2-}$ host. The host framework exhibits a 4-connected diamond topology, and is constructed from $[\text{AlMo}_6\text{H}_6\text{O}_{24}]^{3-}$ clusters connected by Ag^+ cations. When the pH value was increased slightly, compound **2** was obtained with a 1D chain structure built up of Anderson polyoxoanions, Ag-3-Hpya coordination complexes and binuclear sodium clusters. By further increasing the pH value (3.50), compound **3** was isolated as a 2D network in which $[\text{AlMo}_6\text{H}_6\text{O}_{24}]^{3-}$ clusters are linked together by Ag^+ cations and Ag-3-Hpya coordination complexes. Their structural differences reveal that the pH value of the reaction system is the key factor influencing the structure and topology of three compounds. The UV-visible-NIR diffuse reflectivity spectra of **1–3** show that they can be regarded as a wide gap semiconductor. Furthermore, the pyrolysis of **1–3** produces three nanocomposites **1'–3'** composed of silver microparticles dispersed in the metal oxides. The photocatalytic properties of **1'–3'** have been investigated.

Received 23rd October 2013,
Accepted 17th November 2013

DOI: 10.1039/c3dt52987h
www.rsc.org/dalton

Introduction

The design and synthesis of inorganic-organic hybrid materials based on polyoxometalates (POMs) through crystal engineering have become a significant research area owing to their versatile structures, and their potential applications in catalysis, medicine, electronics, magnetism and optics.^{1–4} Some parameters such as initial reactants and their stoichiometry, crystallization temperature and pH value can significantly affect the topological structures and their properties.^{5–8} To address the effect of pH values on the construction of hybrid architectures, many efforts have been made,⁹ because

the pH values of reaction systems can produce different POM structures, adjust the coordination abilities of POMs and metal cations or affect the protonation degrees of organic ligands. So far, research on pH-dependent POM chemistry has mainly focused on the octamolybdate, Keggin and Wells-Dawson POMs. Ma and coworkers reported four copper-based and two cobalt-based octamolybdate hybrid materials with 1,10-(1,4-butanediyl)bis(imidazole) or 1,10-(1,4-butanediyl)bis-[2-(4-pyridyl)benzimidazole] ligands at different pH values.¹⁰ Su *et al.* also isolated six octamolybdate-based hybrids which exhibit either fascinating polythreaded topology or supramolecular isomers with the 1,10-(1,4-butanediyl)bis(imidazole) ligand.¹¹ Long's group successfully reviewed a series of pH-dependent hybrids based on the Keggin anion $[\text{SiW}_{12}\text{O}_{40}]^{4-}$ and the 4,4'-bipy ligand.¹² Cao's group utilized Na_2WO_4 , H_3PO_4 , metal cations and 4,4'-bipy as reactants and got interesting hybrids based on Keggin or Wells-Dawson POMs by adjusting the pH values.¹³ Recently, Peng and coworkers have reported four new hybrids based on Wells-Dawson POMs and Ag^{+} -4,4'-bipy coordination complexes.¹⁴ In contrast, a discussion of the effect of pH values on Anderson POM-based hybrid materials has been rarely reported, although Anderson-type

^aCollege of Chemistry, Dalian University of Technology, Dalian 116023, P. R. China.
E-mail: anh@dlut.edu.cn; Tel: +86-411-84657675

^bCollege of Medical Laboratory, Dalian Medical University, Dalian 116044, P. R. China

†Electronic supplementary information (ESI) available: Selected bond lengths and angles of **1–3** are respectively listed in Table S1. The 3D host-guest frame for **1**, 3D supramolecular framework for **3**, IR spectra, PXRD patterns, TG curves and analysis for **1–3**, EDX for **1'–3'** are available. CCDC 954134–954136. For ESI and crystallographic data in CIF or other electronic format see DOI: [10.1039/c3dt52987h](https://doi.org/10.1039/c3dt52987h)

Polyoxoanions have been demonstrated as many-sided polyoxoanion synthons for the preparation of hybrid frameworks and as effective catalysts for oxidation, hydrogenolysis or photocatalysis reactions.^{15,16} It is thus of considerable interest to investigate the influence of pH values on Anderson POM-based hybrid architectures in crystal engineering.

The selection of the organic ligand is extremely important because the structure of the organic ligand can control and adjust the topologies of POM frameworks. Furthermore, the coordination modes of the ligands are greatly affected by the pH values of reaction solutions, which provide a pathway for designing the final species. Recently, two polymorphs based on Anderson-type POMs in the presence of the pyridylacrylic acid (H₂p_{ya}) ligand have been separated *via* adjusting the pH values of the system by our group.¹⁷ Thus, the bifunctional pyridylacrylic acid ligand is continuously introduced into the synthetic system. On the other hand, silver(I) ion as a labile metal center has attracted considerable attention for its high affinity for N and O donors, versatile coordination behaviors such as linear, T-type, "seesaw", "square pyramidal" and "trigonal bipyramidal" coordination geometries, generally adopting coordination numbers of 2–6 in covalent complexes, and its special photophysical and photochemical properties. So far, some interesting POM-based hybrid compounds modified by Ag⁺ ions have been reported by the research groups of Peng, Lu, Cronin and Hill, respectively.^{18–21} However, the reports on high-dimensional POM-based Ag⁺ complexes are still relatively limited, especially on those combined with Anderson-type POMs.²²

In this paper, three new Anderson POM-based hybrid frames (3-H₂p_{ya})₂[AgAlMo₆H₆O₂₄]·3H₂O **1**, HNa₂[(3-p_{ya})(3-H₂p_{ya})Ag]₂[AlMo₆H₆O₂₄]·8H₂O **2** and [(3-H₂p_{ya})₂Ag]₂[(H₂O)₂Ag]₂[AlMo₆H₆O₂₄]]·2H₂O **3** (3-H₂p_{ya} = 3-(3-pyridyl)acrylic acid) have been synthesized by precisely controlling pH values. Compound **1** represents a rare 3D host–guest frame with a silver coordination complex as a guest molecule; compound **2** is a 1D chain structure; compound **3** is a 2D covalent network. Moreover, the pyrolysis of crystalline precursors **1**–**3** can lead to the formation of three nanocomposites **1'**–**3'** which are composed of silver microparticles with different morphologies dispersed in the resulting molybdenum oxides and aluminum oxides. Nanocomposites **1'**–**3'** show good activity in photocatalyzing the degradation of the organic dye RhB.

Experimental section

Materials and measurements

All chemicals were commercially purchased and used without further purification. Elemental analyses (C, H and N) were performed on a Perkin-Elmer 2400 CHN elemental analyzer; Mo, Al, Ag and Na were analyzed on a PLASMA-SPEC (I) ICP atomic emission spectrometer. IR spectra were recorded in the range 400–4000 cm⁻¹ on an Alpha Centaur FT/IR Spectrophotometer using KBr pellets. TG analyses were performed on a Perkin-Elmer TGA7 instrument in flowing N₂ with a heating rate of

10 °C min⁻¹. Diffuse reflectivity spectra were collected on a finely ground sample using a Cary 500 spectrophotometer equipped with a 110 mm diameter integrating sphere, which were measured from 200 to 800 nm. PXRD patterns of the samples were recorded on a Rigaku Dmax 2000 X-ray diffractometer with graphite monochromatized Cu-K α radiation (λ = 0.154 nm) and 2θ varying from 5 to 60°. UV-vis spectra were acquired using an Analytik Jena SPECORD S600 spectrophotometer equipped with a diode-array detector and an immersible fiber-optic probe. Scanning electron microscopy was performed using a FEI/Quanta 450 system or a FEI/NOVA NanoSEM 450 instrument. Samples were directly deposited on clean silicon wafers.

Synthesis of (3-H₂p_{ya})₂[AgAlMo₆H₆O₂₄]]·3H₂O (1). A sample of Na₂MoO₄·2H₂O (0.581 g, 2.4 mmol) was dissolved in 30 mL water followed by the addition of 3.22 mL glacial acetic acid and 10 mL aqueous solution of Al(NO₃)₃·9H₂O (0.358 g, 0.96 mmol) with stirring. Then, a mixture of 20 mL aqueous solution of AgNO₃ (0.272 g, 0.8 mmol) and 3-H₂p_{ya} (0.18 g, 1.2 mmol) was added. The pH value of the mixture was about 2.50, and the solution was heated for 1 h at 80 °C. The filtrate was kept for three weeks under ambient conditions, after which time colorless rod crystals of **1** were isolated in about 35% yield (based on Ag). Elemental analyses: Calc. for **1**: Mo, 33.64; Al, 1.58; Ag, 12.61; C, 16.83; N, 2.45; H, 1.99 (%). Found: Mo, 33.07; Al, 1.74; Ag, 12.26; C, 16.45; N, 2.61; H, 2.30 (%). FTIR data (cm⁻¹): 3420(s), 3063(s), 1672(s), 1640(m), 1602(m), 1546(w), 1411(m), 1257(m), 1228(m), 1194(m), 941(vs), 907(vs), 814(m), 651(vs), 577(m), 535(m) and 445(m).

Synthesis of HNa₂[(3-p_{ya})(3-H₂p_{ya})Ag]₂[AlMo₆H₆O₂₄]]·8H₂O (2). The synthesis procedure for **2** is similar to **1**, except that the pH value was adjusted to 3.10 by 1 M NaOH. The filtrate was kept for five weeks under ambient conditions, and then colorless triangular block crystals of **2** were isolated in about 25% yield (based on Ag). Elemental analyses: Calc. for **2**: Mo, 28.87; Al, 1.35; Ag, 10.82; Na, 2.31; C, 19.26; N, 2.81; H, 2.46 (%). Found: Mo, 28.72; Al, 1.55; Ag, 10.59; Na, 2.08; C, 19.16; N, 3.01; H, 2.93 (%). FTIR data (cm⁻¹): 3402(s), 2925(w), 2361(w), 1639(s), 1537(m), 1389(s), 1295(m), 1217(m), 1119(w), 979(w), 908(vs), 816(m), 656(vs), 584(m), 532(m) and 446(m).

Synthesis of [(3-H₂p_{ya})₂Ag]₂[(H₂O)₂Ag]₂[AlMo₆H₆O₂₄]]·2H₂O (3). The synthesis procedure for **3** is similar to **1**, just with pH = 3.50. The filtrate was kept for one month under ambient conditions, and then colorless block crystals of **3** were isolated in about 22% yield (based on Ag). Anal. calcd for **3**: Mo, 33.42; Al, 1.57; Ag, 18.79; C, 11.14; N, 1.63; H, 1.86 (%). Found: Mo, 33.30; Al, 1.85; Ag, 18.48; C, 10.85; N, 1.81; H, 2.03 (%). FTIR data (cm⁻¹): 3421(s), 2926(w), 1994(w), 1642(s), 1537(s), 1395(s), 1294(w), 1210(w), 1050(w), 911(vs), 651(vs), 578(m), 532(m) and 442(m).

X-ray crystallography

The crystallographic data of three compounds were collected using the Bruker Smart CCD diffractometer with Mo K α radiation (λ = 0.71073 Å) by ω and θ scan modes. Empirical

Table 1 Crystal data and structure refinement for **1–3**

Complex	1	2	3
Formula	$C_{24}H_{34}Ag_2AlMo_6N_3O_{33}$	$C_{32}H_{49}Ag_2AlMo_6Na_2N_4O_{40}$	$C_{16}H_{32}Ag_3AlMo_6N_2O_{34}$
Formula weight	1710.90	1994.09	1722.67
T (K)	293(2)	220	293(2)
Crystal system	Orthorhombic	Monoclinic	Triclinic
Space group	$Fdd\bar{d}$	$P2(1)/c$	$P\bar{1}$
a (Å)	15.892(2)	9.8882(2)	10.0978(8)
b (Å)	29.617(4)	24.4954(5)	10.5238(8)
c (Å)	37.798(6)	12.1347(2)	10.7062(8)
α (°)	90	90	87.9400(10)
β (°)	90	101.6530(1)	73.8280(10)
γ (°)	90	90	63.0990(10)
U (Å ³)	17 790(5)	2878.63(1)	969.05(13)
Z	16	2	1
μ (mm ⁻¹)	2.624	2.068	3.494
Reflections collected	21 439	19 102	5533
Independent reflections	3926	5064	3356
R (int)	0.0325	0.0258	0.0122
GOF on F^2	1.129	1.096	1.076
$R_1^a [I > 2\sigma(I)]$	0.0359	0.0354	0.0226
$wR_2^b [I > 2\sigma(I)]$	0.0882	0.0926	0.0599
R_1 (all data)	0.0415	0.0372	0.0244
wR_2 (all data)	0.0914	0.0939	0.0611

$$^a R_1 = \sum ||F_o| - |F_c|| / \sum |F_o|, ^b wR_2 = \sum [w(F_o^2 - F_c^2)^2] / \sum [w(F_o^2)^2]^{1/2}.$$

absorption correction was applied. The structures of **1–3** were solved by the direct method and refined by the Full-matrix least squares on F^2 using the SHELXTL-97 software.²³ All of the non-hydrogen atoms were refined anisotropically in **1–3**. The hydrogen atoms attached to isolated water molecules were located from the electron density map in **1–3**, and those attached to the disordered water molecules were not located. Positions of the hydrogen atoms attached to carbon atoms and those attached to nitrogen atoms were fixed in ideal positions. Site occupancies of the partial crystal water molecules in **1** and **2** were set to be less than 1 through the refinement of their thermal parameters due to disorder. Compound **1** contains disordered carboxyl oxygen atom O13 and O13A. Compound **2** also contains disordered carboxyl oxygen atom O15 and O15A. Other restraints such as ‘isor’ or ‘dfix’ were used in the refinements for obtaining reasonable atom sites and thermal parameters. A summary of the crystallographic data and structural determination for **1–3** is provided in Table 1.

CCDC reference number: 954135 for **1**, 954136 for **2** and 954134 for **3**.

Results and discussion

Synthesis

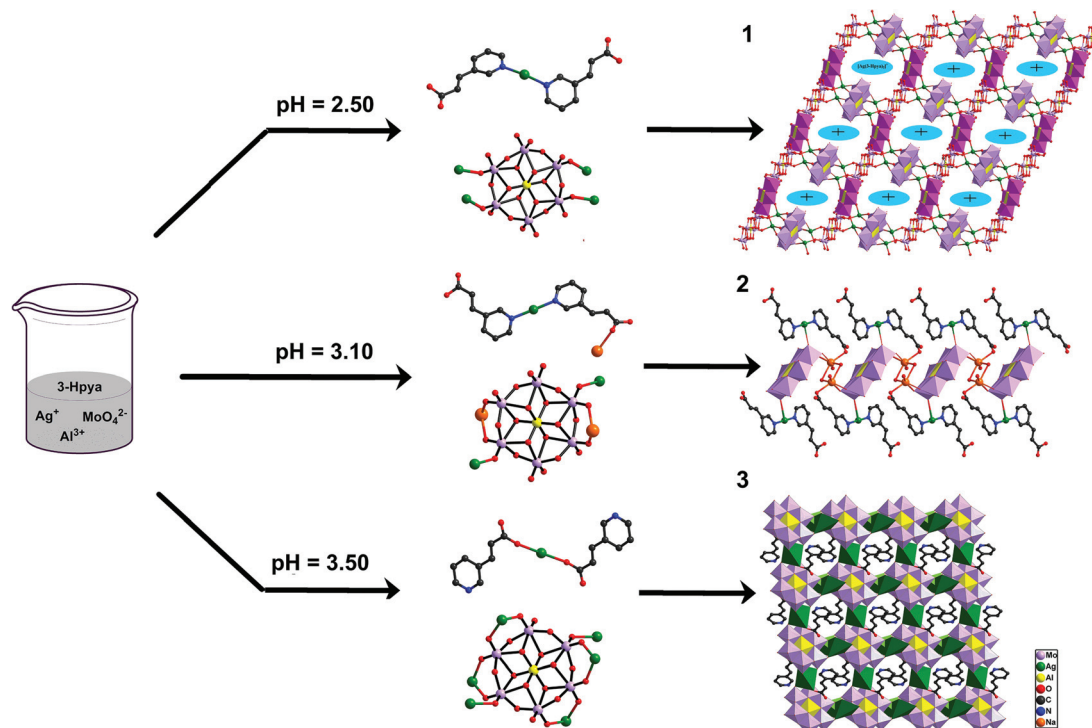
The reactivity of Na_2MoO_4 , $Al(NO_3)_3$ and the Ag^+ cation in the presence of the pyridylacrylic acid ligand has been investigated. Three compounds were obtained (Scheme 1). Compounds **1–3** were synthesized under the same reaction conditions, except for the alternation of pH values. It is clear that the pH value of the reaction system is the key factor influencing the structures and topologies of these compounds. At lower pH values, compound **1** is isolated, exhibiting a 3D

covalent frame with 4-connected diamond topology; with an increase of the pH value, 1D chain structure and 2D network are formed, respectively.

Based on the structures of **1–3**, we found that the pH influence on the structure is, in fact, its effect on degree of the deprotonation of 3-Hpya as well as the coordination modes of 3-Hpya.²⁴ The high pH value favors the deprotonation of the 3-Hpya, while deprotonation of the 3-Hpya can promote its coordination to the Ag^+ ion on the basis of acid–base chemistry and soft and hard acid–base principle (Scheme S1†). At pH = 2.50, one of two unique 3-Hpya molecules is protonated, restricting itself to coordinate to the Ag^+ ion in **1**. Thus, some Ag^+ cations are coordinated to 3-Hpya molecules to produce Ag –3-Hpya coordination complexes, while other Ag^+ cations linked the Anderson POMs $[AlMo_6H_6O_{24}]^{3-}$ to form a 3D architecture. When the pH value was adjusted to 3.10, compound **2** was obtained. In **2**, all the nitrogen atoms of 3-Hpya ligands are nonprotonated. Ag^+ cations linked the 3-Hpya ligands to form coordination complexes. Then, Ag –3-Hpya coordination fragments are anchored on the terminal oxygen atoms of the $[AlMo_6H_6O_{24}]^{3-}$ POM to yield a bi-supporting subunit, which can be joined by sodium dimers to produce a 1D chain. When the pH value reached 3.50, carboxyl oxygen atoms of 3-Hpya are deprotonated to coordinate to Ag^+ cations and give **3** a 2D sheet. For a higher pH ($pH > 4.0$), only a mass of precipitates appear, which may be due to the free Ag^+ readily transformed to Ag_2O at a higher pH value. In a word, the pH effects are responsible for the structural diversity of the resultant Anderson POM-based hybrids.

Crystal structure of **1**

The single crystal X-ray diffraction analysis shows that compound **1** displays a 3D open framework composed of



Scheme 1 Schematic representation of three Anderson POM-based hybrid architectures synthesized at the different pH values.

$[\text{AlMo}_6\text{H}_6\text{O}_{24}]^{3-}$ polyoxoanions and Ag^+ cations, with silver coordination complexes, protonated 3-Hpya molecules and lattice water molecules as guests. Each $[\text{AlMo}_6\text{H}_6\text{O}_{24}]^{3-}$ cluster has a typical B-type Anderson structure, which is made up of seven edge-sharing octahedra, six of which are $\{\text{MoO}_6\}$ octahedra arranged hexagonally around the central $\{\text{Al}(\text{OH})_6\}$ octahedron. Four kinds of oxygen atoms exist in the cluster: terminal oxygen O_{t} , terminal oxygen $\text{O}_{\text{t}'}$ linked to Ag^+ , double-bridging oxygen O_{b} and central oxygen O_{c} . Thus the Mo–O bond lengths fall into four classes: Mo– O_{t} 1.701(5)–1.725(4) Å, Mo– $\text{O}_{\text{t}'}$ 1.712(4)–1.717(4) Å, Mo– O_{b} 1.901(4)–1.951(4) Å and Mo– O_{c} 2.291(4)–2.329(4) Å in **1**. The central Al– O_{c} distances vary from 1.889(4) to 1.913(4) Å in **1**, with a mean value of 1.901 Å. The bond angles of $\text{O}-\text{Al}-\text{O}_{\text{cis}}$ range from 85.05(2) to 94.95(2)°, and $\text{O}-\text{Al}-\text{O}_{\text{trans}}$ is 180.00°. All of the bond lengths and bond angles are within the normal ranges and are consistent with those described in the literature.²⁵

The asymmetric unit in **1** consists of one crystallographically independent “half” Anderson anion, two halves of crystallization-independent Ag^+ cations and one 3-Hpya ligand (Fig. 1a). Unique $\text{Ag}(1)$ cation (disordered $\text{Ag}1$ ion over two positions with half-occupancy), has a distorted tetrahedral environment, being coordinated by four terminal oxygen atoms from four $[\text{AlMo}_6\text{H}_6\text{O}_{24}]^{3-}$ units [$\text{Ag}-\text{O}$ 2.290(4) and 2.389(4) Å]. The $\text{Ag}(2)$ just existing as an isolated metal–organic coordination complex, adopts a linear geometry, being defined by two N atoms from two 3-Hpya ligands with the $\text{Ag}-\text{N}$ distance of 2.098(5) Å. There are two crystallographically independent 3-Hpya molecules. One acts as a monodentate

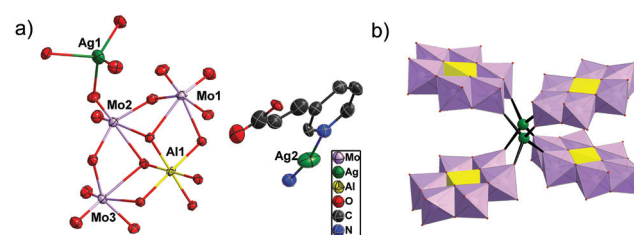


Fig. 1 (a) ORTEP drawing of **1** with thermal ellipsoids at 50% probability. (b) Polyhedral and ball-stick representation of the coordination modes of $\text{Ag}(1)$ coordination unit and $[\text{AlMo}_6\text{H}_6\text{O}_{24}]^{3-}$ anion in **1** (color code: Al, yellow; Mo, pink; Ag, green; O, red).

ligand coordinated to one Ag^+ cation to yield an Ag-3-Hpya fragment, and the other as an isolated organic molecule. In the IR spectrum of compound **1**, the features at 1672 and 1412 cm^{-1} can be regarded as characteristics of the 3-Hpya molecule (Fig. S5a†).

As shown in Fig. 2a, firstly the $[\text{AlMo}_6\text{H}_6\text{O}_{24}]^{3-}$ clusters are linked by some Ag^+ ions to form a 1D chain, and then each chain is connected to two other parallel chains through $[\text{AlMo}_6\text{H}_6\text{O}_{24}]^{3-}$ polyoxoanions to yield a window-like 2D layer (Fig. 2b). Furthermore, these 2D sheets are pillared by other $[\text{AlMo}_6\text{H}_6\text{O}_{24}]^{3-}$ polyoxoanions to produce a 3D open framework (Fig. 3a). It is notable that this kind of connection mode results in the formation of a 1D channel. The dimensions of the channel are about 12.6 × 8.5 Å along the [1 0 1] direction. These channels are formed around a cationic silver-3-Hpya coordination group, which does not only act as a charge-

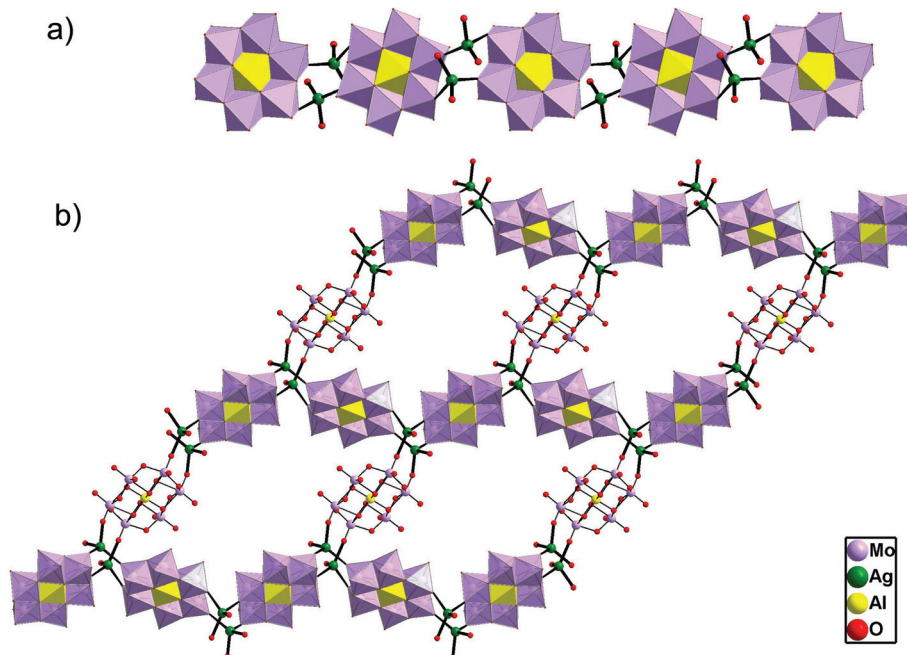


Fig. 2 (a) Polyhedral and ball-stick view of the 1D linear chain in **1**. (b) 2D sheet of **1**, showing the 1D chains linked by other $[\text{AlMo}_6\text{H}_6\text{O}_{24}]^{3-}$ anions (color code: Al, yellow; Mo, pink; Ag, green; O, red).

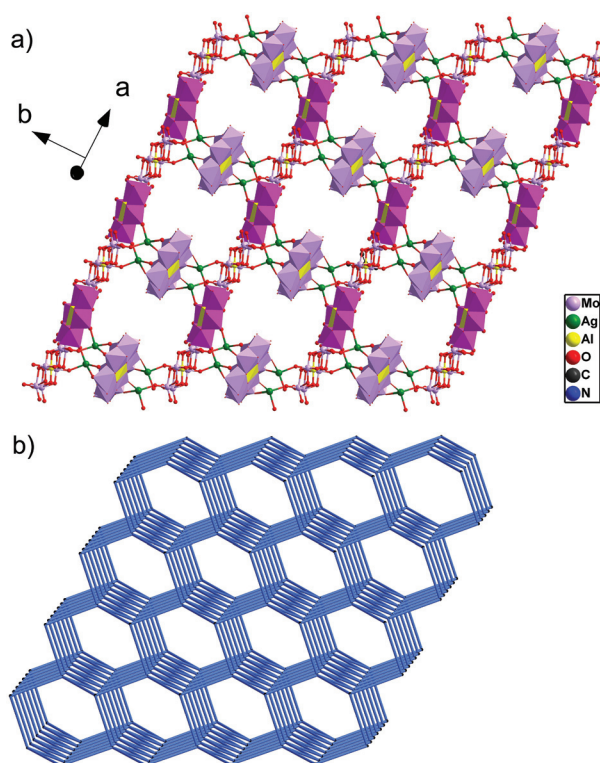


Fig. 3 (a) A view along the [1 0 1] axis illustrating the 3D open framework with 1D channels in **1** (color code: Al, yellow; Mo, pink/purple; Ag, green; O, red). Ag-3-Hpya coordination fragments, free 3-Hpya and water molecules situated in the channels are omitted for clarity. (b) Schematic representation of the 4-connected diamond topology of **1**.

balancing unit but directs the formation of the porous structure by templating the channels (shown in Fig. S2†). Intriguingly, metal coordination complex cations are often used in the templated synthesis of zeolites;²⁶ however, compound **1** represents a very rare example of 3D covalent POM framework with metal coordination complexes as a guest template. A better insight into the nature of such 3D framework can be achieved by reducing the multidimensional structure to a simple node and linker net. According to the simplification principle, the Ag(1) center is defined as a 4-connected node and the $[\text{AlMo}_6\text{H}_6\text{O}_{24}]^{3-}$ ligating with two Ag(1) centers serves as a linker. Therefore, the resulting 3D frame is a uninodal 4-connected diamond-related net with Schläfli symbol of 6^6 , as shown in Fig. 3b.

Crystal structure of **2**

The preparation of compound **2** was similar to that of compound **1** except that the pH value was adjusted to about 3.10. The single crystal X-ray diffraction analysis reveals that compound **2** exhibits a 1D chain structure composed of $[\text{AlMo}_6\text{H}_6\text{O}_{24}]^{3-}$ polyoxoanions, binuclear sodium clusters and Ag-3-Hpya coordination complexes. The $[\text{AlMo}_6\text{H}_6\text{O}_{24}]^{3-}$ polyoxoanion is also a B-type Anderson structure, similar to compound **1**. Five kinds of oxygen atoms exist in the cluster according to the manner of oxygen coordination, that is terminal oxygen O_{t} , terminal oxygen $\text{O}_{\text{t}'}$ linked to Ag^+ , terminal oxygen $\text{O}_{\text{t}''}$ linked to Na^+ , double-bridging oxygen O_{b} and central oxygen O_{c} . Thus the Mo-O distances can be grouped into five sets: Mo- O_{t} 1.709(4)–1.721(4) Å, Mo- $\text{O}_{\text{t}'}$ 1.711(4) Å,

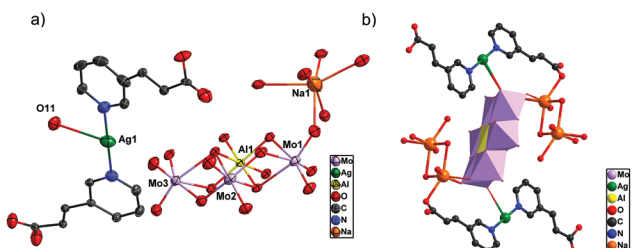


Fig. 4 (a) ORTEP drawing of compound 2 with thermal ellipsoids at 50% probability. Isolated molecules are omitted for clarity. (b) Polyhedral and ball-stick view of one Anderson polyoxoanion linked by two Ag-3-Hpya complexes and two sodium dimers in 2 (color code: Al, yellow; Mo, pink; Ag, green; Na, orange; O, red; N, blue; C, grey).

Mo–Ot' 1.706(4)–1.710(4) Å, Mo–Ob 1.911(4)–1.948(3) Å and Mo–Oc 2.287(3)–2.322(3) Å in 2. The central Al–Oc distances vary from 1.875(3) to 1.923(3) Å in 2, with a mean value of 1.900 Å. The bond angles of O–Al–O_{cis} range from 85.00(1) to 95.07(1)°, and O–Al–O_{trans} is 180.00°, similar to 1.

The asymmetric unit in the structure of 2 consists of one crystallographically independent “half” Anderson anion, one sodium cation and one {Ag(3-Hpya)} coordination complex (see Fig. 4a). There is one crystallization-independent Ag cation in the complex unit. Ag(1) bonded to one polyoxoanion as a supporter, adopts a T-type geometry, being defined by two nitrogen atoms from two 3-Hpya molecules [Ag–N 2.160(4) and 2.162(4) Å], and one terminal oxygen atom from one [AlMo₆H₆O₂₄]³⁻ unit [Ag–O 2.770(4) Å]. Crystallographically unique Na(1) atom links with two terminal oxygen atoms from one [AlMo₆H₆O₂₄]³⁻ unit [Na–O 2.372(5) and 2.584(5) Å], one carboxyl oxygen atom from one 3-pya molecule [Na–O 2.526(5) Å], and three water molecules to finish its octahedral coordination environment. The average Na–O bond length is 2.374 Å. Two coordinated water molecules can bridge two adjacent Na atoms to form a sodium dimer. There are two crystallographically independent 3-Hpya molecules. The “acrylic acid” fragment in one ligand was found to be disordered with two different orientations. This kind of disorder phenomenon has been observed in the Ag-pyridylacrylic acid coordination complex.²⁷ The disordered one acts as a monodentate ligand coordinated to one Ag⁺ cation to form a {Ag(3-Hpya)₂} fragment by pyridine nitrogen atoms, and the other as a bidentate ligand coordinated to one Ag⁺ cation and one Na⁺ cation. In the IR spectrum of compound 2, the features at 1639 and 1389 cm⁻¹ can be regarded as characteristics of the 3-Hpya molecule (Fig. S5b†).

In the structure of 2, two {Ag(3-Hpya)₂} coordination complexes are firstly anchored on the terminal oxygen atoms of one [AlMo₆H₆O₂₄]³⁻ polyoxoanion to form a bi-supporting structure, then these bi-supporting subunits are interconnected to generate a 1D chain by the sodium dimers (shown in Fig. 5a). A similar dimer built up of two sodium cations and water molecules has been observed in other Ag linked POM hybrids.^{22a} Then, adjacent 1D chains are linked up to yield a 2D lamellar structure by strong hydrogen-bonding interactions

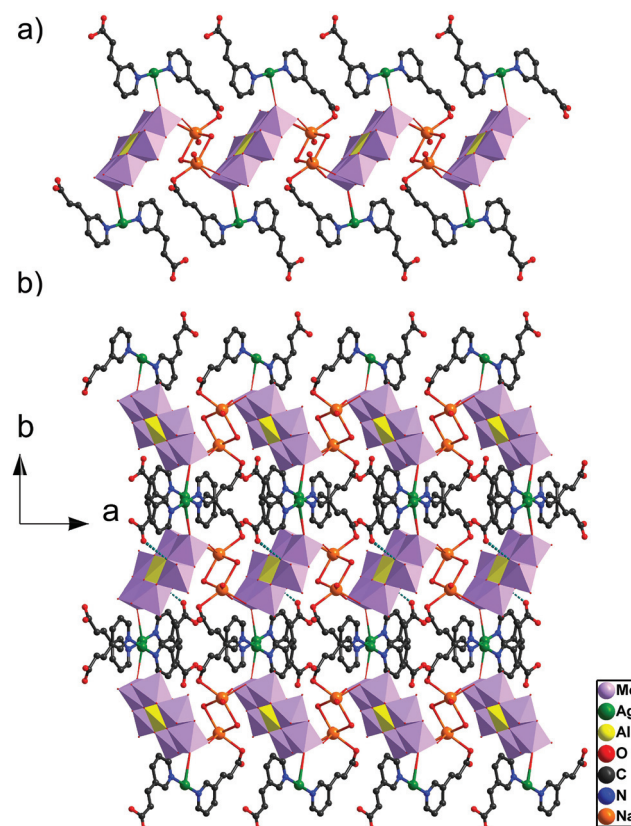


Fig. 5 (a) Polyhedral and ball-stick view of the 1D chain in 2. (b) 2D supramolecular lamellar structure of 2 through the hydrogen-bonding interactions, and face-to-face π - π stacking interactions (color code: Al, yellow; Mo, pink; Ag, green; Na, orange; O, red; N, blue; C, grey).

(O₃…O₁₆ 2.753 Å) between central oxygen atoms of polyoxoanions and carboxyl oxygen atoms of ligands, and face-to-face π - π stacking interactions (3.64 Å) between benzene rings of adjacent organic ligands (Fig. 5b). Free water molecules are filled in the cavities of supramolecular structures and participate in the extensive hydrogen-bonding interactions with the polyoxoanion framework.

Crystal structure of 3

The preparation of compound 3 was similar to those of 1 and 2 except that the pH value was adjusted to about 3.50. The single-crystal X-ray analysis reveals that the structure of compound 3 exhibits a 2D layer assembled by [AlMo₆H₆O₂₄]³⁻ polyoxoanions, Ag⁺ cations and Ag-3-Hpya complexes. The [AlMo₆H₆O₂₄]³⁻ cluster is also a B-type Anderson structure. Four kinds of oxygen atoms exist in the cluster according to the manner of oxygen coordination, similar to compound 1. Thus the Mo–O distances can be grouped into four sets: Mo–Ot 1.702(3) Å, Mo–Ot' 1.708(3)–1.725(3) Å, Mo–Ob 1.910(2)–1.954(2) Å and Mo–Oc 2.241(2)–2.337(2) Å in 3. The central Al–Oc distances vary from 1.885(2) to 1.914(2) Å in 3, with a mean value of 1.901 Å. The bond angles of O–Al–O_{cis} range from 84.37(1) to 95.63(1)°, and O–Al–O_{trans} is 180.00°, similar to 1 and 2.

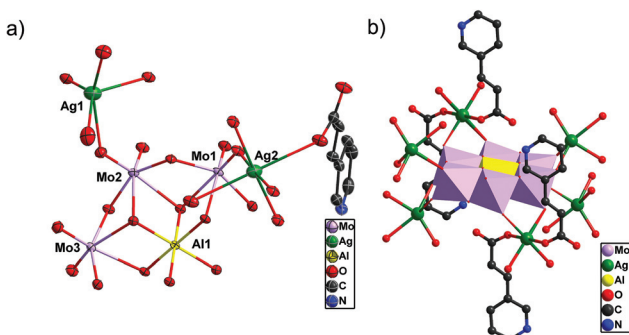


Fig. 6 (a) ORTEP drawing of **3** with thermal ellipsoids at 50% probability. H atoms and crystal water molecules are omitted for clarity. (b) Polyhedral and ball-stick representation of the Anderson polyoxoanion $[AlMo_6H_6O_{24}]^{3-}$ and its coordination environment in **3** (color code: Al, yellow; Mo, pink; Ag, green; O, red).

The asymmetric unit in the structure of **3** consists of one crystallographically independent “half” Anderson-type anion linked up by one Ag^+ ion and half Ag^+ coordination complex (see Fig. 6a). Interestingly, Al(1) and Ag(2) atoms lie on independent crystallographic inversion centers. The unique Ag(1) is five-coordinate, defined by three terminal oxygen atoms from two $[AlMo_6H_6O_{24}]^{3-}$ units ($Ag(1)-O$ 2.314(3), 2.429(3) and 2.557(3) Å), and two water molecules ($Ag(1)-OW$ 2.267(3) and 2.639(3) Å). Each crystallographically half-occupied Ag(2) ion is in an octahedron geometry, coordinated by four terminal oxygen atoms from two $[AlMo_6H_6O_{24}]^{3-}$ units ($Ag(2)-O$ 2.374(3) and 2.447(3) Å), and two carboxyl oxygen atoms from two 3-Hpya molecules ($Ag(2)-O$ 2.741(3) Å). One crystallographically independent 3-Hpya molecule acts as a monodentate ligand, coordinating to one Ag(2) atom by one carboxyl oxygen atom (Fig. 6b). In the IR spectrum of compound **3**, the features at 1642 and 1395 cm⁻¹ can also be regarded as characteristics of the 3-Hpya molecule (Fig. S5c†). The difference between $\nu_{as}(CO^{2-})$ and $\nu_s(CO^{2-})$ in the IR spectrum has been successfully used to derive information regarding bonding modes of carboxylate anions.²⁸ The $\Delta\nu$ of 247 cm⁻¹ indicates the monodentate coordination mode of the carboxylate group in **3**, which is consistent with the results of the X-ray analysis.

The structural feature of **3** is that these Anderson-type POMs are linked together by Ag^+ cations to yield a 1D linear chain as shown in Fig. 7a. This kind of 1D chains are further connected by Ag-3-Hpya fragments to produce a novel 2D network (Fig. 7b). Compound **3** represents a rare example of 2D hybrid architectures based on Anderson-type POMs and silver-organic complexes. Each Anderson POM unit acts as a hexa-dentate ligand coordinating to four Ag(1) and two Ag(2) cations through the terminal oxygen atoms in the 2D structure. From the view of topology, this 2D sheet is a common 4-connected 4⁴ net with Anderson-type POM units as nodes and the Ag^+ ions and Ag-3-Hpya complexes as linkers (see Fig. S3†). Then, these 2D layers are packed together to form a 3D supramolecular architecture *via* weak hydrogen-bonding interactions between carbon atoms of 3-Hpya molecules and

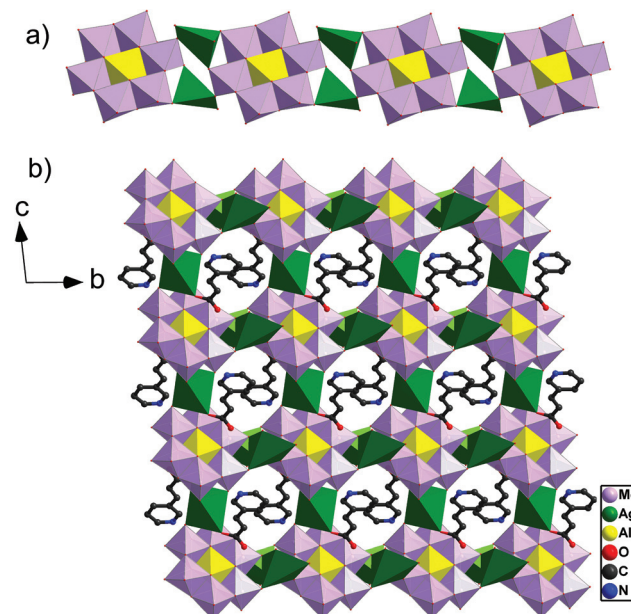


Fig. 7 (a) Polyhedral view of the 1D linear chain in **3**. (b) 2D sheet of **3**, showing the 1D inorganic chains linked by Ag-3-Hpya coordination complexes (color code: Al, yellow; Mo, pink; Ag, green; O, red).

oxygen atoms of polyoxoanions ($C_2-H\cdots O_8 = 3.160$ Å; $C_6-H\cdots O_9 = 3.195$ Å; $C_8-H\cdots O_7 = 3.248$ Å) (see Fig. S4†).

Bond valence sum calculations²⁹ show that all Mo atoms are in the +6 oxidation state, Al atoms are in the +3 oxidation state, and Ag sites are in the +1 oxidation state. These results are consistent with the charge balance considerations.

Optical band gap

To investigate the conductivity potentials of compounds **1–3**, the diffuse reflectivity for solid samples of **1–3** were measured to obtain the band gap (E_g). The phase purities of three solid samples have been characterized by PXRD (Fig. S6†). The absorption (α/S) data were calculated from the reflectivity using the Kubelka-Munk function: $\alpha/S = (1 - R)^2/2R$, where R is the reflectivity at a given wavelength, α is the absorption coefficient, and S is the scattering coefficient. The band gap was determined as the intersection point between the energy axis at $\alpha/S = 0$ and the line extrapolated from the linear portion of the adsorption edge in a plot of α/S against energy E . The α/S versus E plots are shown in Fig. 8. For compounds **1–3**, the well-defined optical absorption associated with band gaps (E_g) can be assessed at 3.10, 3.28 and 2.78 eV, respectively. The reflectance spectra imply that compounds **1–3** are potential semiconductors with wide band gaps. In addition, the optical band gap has been measured for the 3-Hpya ligand (Fig. S7†). The E_g value of the ligand is 3.64 eV, which is much higher than those of **1–3**. Therefore, the optical band gaps of **1–3** are not relevant to the 3-Hpya ligands, but the Anderson POM $[AlMo_6H_6O_{24}]^{3-}$ and silver cation.³⁰ A similar phenomenon has been observed in several Lindqvist or octamolybdate-based inorganic-organic hybrid solids, such as $(n\text{-Bu}_4N)_2[Mo_6O_{17}(\equiv NAr)_2]$ ($Ar = o\text{-CH}_3OC_6H_4$) ($E_g = 2.25$ eV), and $[Cd$

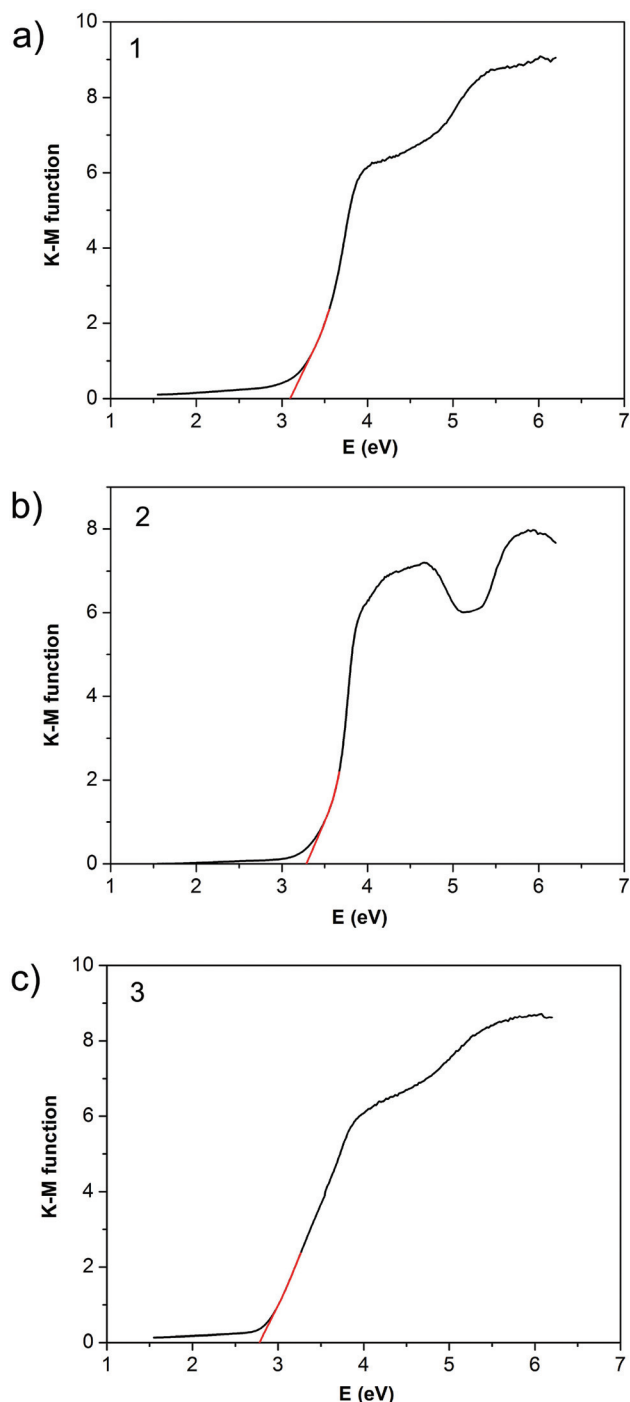


Fig. 8 UV-vis-NIR diffuse reflectance spectra of K-M functions vs. energy (eV) of compounds **1–3**.

$(BPE)(\alpha\text{-Mo}_8O_{26})][Cd(BPE)(DMF)_4]\cdot 2DMF$ ($E_g = 3.45$ eV).³¹ Moreover, a variety of E_g values suggests that the optical band gaps of POM-based hybrids could be tuned effectively *via* different connectivity between polyoxoanions and metal coordination units.

SEM images

The thermal stabilities of three compounds are investigated by TG analysis in a N_2 stream (see Fig. S8a–8c†). The TG curves of

these compounds indicate that they start to decompose below 70 °C. The TG results and the residue of the amorphous oxide and crystalline silver metal enable us to investigate their nano-scale morphologies after treatment at 1000 °C.

SEM images of the residues indicate that the Ag(0) micro-particles monodisperse in molybdenum oxides and slight aluminum oxides (sodium oxides only existing in **2'**) to form three nanocomposites **1'–3'**. Energy-dispersive X-ray (EDX) spectra of three nanocomposites are depicted in Fig. S9† for clearly showing the existence of Ag, Mo, Al and O (Na only in **2'**) in the final product. Interestingly, the Ag microparticles and molybdenum oxides of three nanocomposites exhibit different morphologies as shown in Fig. 9. For **1'**, the molybdenum oxide displays a plane matrix with spherical metallic silver microparticles adhering to its surface; for **2'** the molybdenum oxide shows nanowire features, and the hexagonal silver plates dispersed in them; for **3'** the molybdenum oxide possesses an amorphous structure with embedded spherical silver microparticles. Xia's group has reported that the morphology and dimensions of Ag nanoparticles strongly depend on reaction conditions such as temperature, the concentration of the Ag^+ cation, and the molar ratio between the repeating unit of organic molecules and Ag^+ .³² In compounds **1–3**, in addition to the discrepant molar ratio between the Ag^+ cation and the 3-Hpya molecule, the concentration and coordination modes of Ag^+ in three solid structures are entirely different, which may be the reason that resulted in Ag microparticles with different morphologies, as the precursors are heated to decompose. Furthermore, as described in the literature,^{33,34} the morphologies and the scale of the nano-species were all associated with the motifs and the interactions among the motifs in their crystals. In compounds **1–3**, Anderson polyoxomolybdate, the Ag^+ cation and the 3-Hpya ligand are joined together by different linking modes to respectively exhibit 3D, 1D and 2D structure owing to the alteration of synthetic pH values, so molybdenum oxides with different morphologies were obtained. As there is no other electron source due to the cluster being fully oxidized, we tentatively postulate that the Ag^+ centers on the initial cluster units are reduced to Ag(0) as electrons are released from cluster framework oxygen ligands, which are then eliminated as molecular oxygen. Such phenomena have been reported in Ag-polyoxotungstate species.³⁵ So far, only Cronin's group and Lu's group have adopted the pyrolysis method to prepare silver microparticles embedded in the tungsten oxides with crystalline Ag-polyoxotungstate precursors, respectively.^{35,36} Herein, we further show that this pyrolysis approach is effective to lead to a new class of Ag-doped molybdenum oxide nanocomposites with a range of interesting physical properties.

Photocatalytic activity

The photocatalytic properties of three nanocomposites **1'–3'** have been investigated with photodegradation of rhodamine B (RhB). In a typical process, 5 mg of sample was dispersed in 100 mL RhB solution (2×10^{-5} mol L⁻¹), and the suspension was magnetically stirred in the dark for 30 min to ensure the

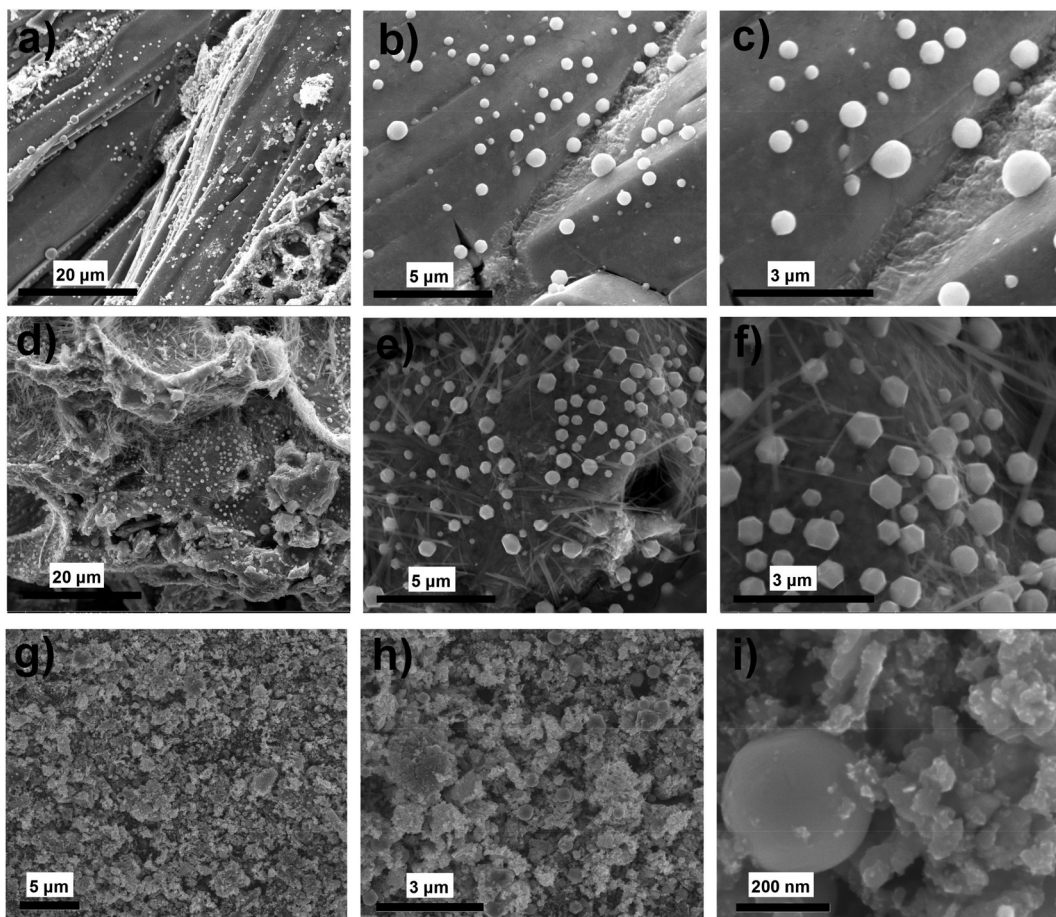


Fig. 9 SEM micrographs of the nanostructure in compounds **1–3** following heating under nitrogen to 1000 °C. (a–c) Display the spherical silver microparticles adhered to the surface of molybdenum oxide matrixes in nanocomposite **1'**. (d–f) Show the hexagonal silver nanoplates dispersed in the molybdenum oxide nanowires in nanocomposite **2'**. (g–i) Exhibit the spherical silver microparticles embedded in the amorphous molybdenum oxides in nanocomposite **3'**.

equilibrium of the working solution. Then the solution was exposed to UV irradiation from a Hg lamp, and kept under stirring during irradiation. A sample was taken out every 1 h for analysis. The evolution of the spectral changes taking place during the photodegradation of RhB over **1'–3'** is shown in Fig. 10. It can be clearly seen that the absorbance peaks of RhB are decreased obviously for **1'–3'** with increasing reaction time. The calculations reveal that the conversions of RhB are 93.7% for **1'**, 94.5% for **2'** and 90.2% for **3'** after 9 h. In comparison, the absorption peaks of RhB without any catalyst show no obvious change (Fig. S10†). The results indicate that nanocomposites **1'–3'** show excellent photocatalytic activities for the degradation of RhB. Under the same condition, crystalline compound **1** as a representative and the salt $(\text{NH}_4)_3[\text{AlMo}_6\text{H}_6\text{O}_{24}]$ of the same weight were used to photocatalytically decompose the RhB, resulting in a drop in the RhB concentrations by 57.0% and 28.4% after 9 h, respectively (Fig. S11, S12†). The salt $(\text{NH}_4)_3[\text{AlMo}_6\text{H}_6\text{O}_{24}]$ exhibited weak photocatalytic activity in the degradation of RhB, so the introduction of the Ag^+ cation into the $[\text{AlMo}_6\text{H}_6\text{O}_{24}]^{3-}$ framework can play the role of improving the photocatalytic activity. Furthermore,

the catalytic effect of compound **1** is not as high as the nanocomposites **1'–3'** (Fig. S13†). The better catalytic results of **1'–3'** may be attributed to the synergistic actions between silver microparticles and metal oxides. Nanocomposites **1'–3'** as heterogeneous catalysts can be easily recovered by simple centrifugal separation.

Conclusions

In summary, we report three Anderson-type POM-based hybrid materials with respective 3D host-guest, 1D chain and 2D layer structures by adjusting the pH values of initial reaction solutions. The successful isolations of **1–3** show us a perspective of extending the POM family through reasonably controlling the reaction pH values. Three hybrid architectures possess different optical band gaps (E_g) owing to different connectivity between Anderson POMs and silver coordination units. Furthermore, pyrolysis of these crystalline compounds **1–3** at elevated temperatures gives rise to nanocomposites **1'–3'** comprising silver microparticles with different morphologies

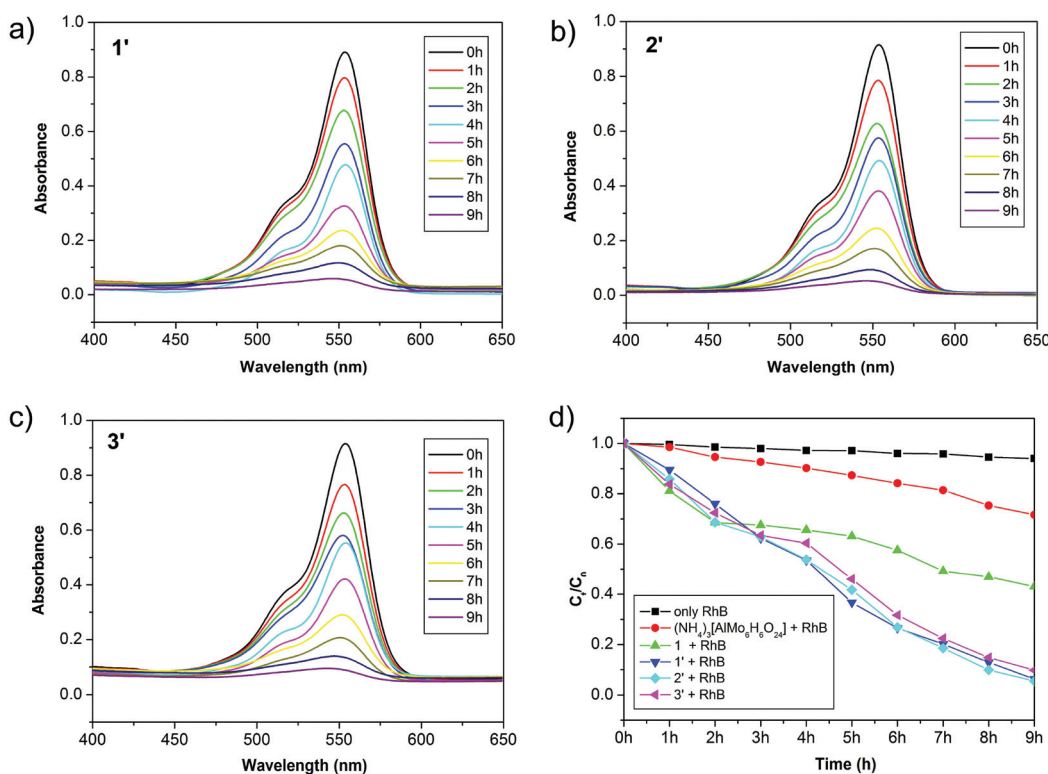


Fig. 10 (a) Absorption spectra of the RhB solution during the decomposition reaction under UV irradiation in the presence of nanocomposite 1'. (b) Absorption spectra of the RhB solution during the decomposition reaction with catalyst 2'. (c) Absorption spectra of the RhB solution during the decomposition reaction with catalyst 3'. (d) Photocatalytic decomposition rate of the RhB solution under UV irradiation with the use of $(\text{NH}_4)_3[\text{AlMo}_6\text{O}_{24}]$, compound 1, nanocomposites 1'–3' and only RhB.

dispersed in the molybdenum and aluminum oxides, respectively. Nanocomposites 1'–3' exhibit excellent photocatalytic activities for the degradation of RhB. This work would shed new light on the development of new nanomaterials from crystalline POM hybrid frameworks for important applications in catalysis.

Acknowledgements

The authors thank the National Natural Science Foundation of China (21371027, 20901013) and Fundamental Research Funds for the Central Universities (DUT12LK01) for financial supports.

Notes and references

- (a) M. T. Pope and A. Müller, *Polyoxometalate Chemistry: From Topology via Self-Assembly to Applications*, Kluwer, Dordrecht, The Netherlands, 2001; (b) V. Soghomonian, Q. Chen, R. C. Haushalter, J. Zubieta and C. J. O'Connor, *Science*, 1993, **259**, 1596; (c) M. A. Al Damen, J. M. Clemente-Juan, E. Coronado, C. Martí-Gastaldo and A. Gaita-Arino, *J. Am. Chem. Soc.*, 2008, **130**, 8874; (d) D. L. Long, E. Burkholder and L. Cronin, *Chem. Soc. Rev.*, 2007, **36**, 105.

2 (a) Q. S. Yin, J. M. Tan, C. Besson, Y. V. Geletii, D. G. Musaev, A. E. Kuznetsov, Z. Luo, K. I. Hardcastle and C. L. Hill, *Science*, 2010, **328**, 342; (b) T. Yamase and M. T. Pope, *Polyoxometalate Chemistry for Nano-Composite Design*, Kluwer, Dordrecht, The Netherlands, 2002; (c) N. Mizuno and M. Misisono, *Chem. Rev.*, 1998, **98**, 199.

3 (a) J. Zhang, J. Hao, Y. G. Wei, F. P. Xiao, P. C. Yin and L. S. Wang, *J. Am. Chem. Soc.*, 2010, **132**, 14; (b) C. Y. Sun, S. X. Liu, D. D. Liang, K. Z. Shao, Y. H. Ren and Z. M. Su, *J. Am. Chem. Soc.*, 2009, **131**, 1883; (c) E. Cadot, M. N. Sokolov, V. P. Fedin, C. Simonnet-Jégat, S. Floquet and F. Sécheresse, *Chem. Soc. Rev.*, 2012, **41**, 7335.

4 (a) S. T. Zheng and G. Y. Yang, *Chem. Soc. Rev.*, 2012, **41**, 7623; (b) A. Banerjee, B. S. Bassil, G. Röschenthaler and U. Kortz, *Chem. Soc. Rev.*, 2012, **41**, 7590; (c) J. Y. Niu, J. A. Hua, X. Ma and J. P. Wang, *CrystEngComm*, 2012, **14**, 4060; (d) Y. Z. Wang, H. L. Li, C. Wu, Y. Yang, L. Shi and L. X. Wu, *Angew. Chem., Int. Ed.*, 2013, **52**, 4577.

5 (a) X. L. Wang, D. Zhao, A. X. Tian and J. Ying, *CrystEngComm*, 2013, **15**, 4516; (b) D. B. Dang, Y. N. Zheng, Y. Bai, X. Y. Guo, P. T. Ma and J. Y. Niu, *Cryst. Growth Des.*, 2012, **12**, 3856.

6 (a) S. Reinoso, M. H. Dickman, M. Reicke and U. Kortz, *Inorg. Chem.*, 2006, **45**, 9014; (b) M. Zhu, S. Q. Su, X. Z. Song, Z. M. Hao, S. Y. Song and H. J. Zhang, *CrystEngComm*, 2012, **14**, 6452.

- 7 K. Yu, B. B. Zhou, Y. Yu, Z. H. Su, H. Y. Wang, C. M. Wang and C. X. Wang, *Dalton Trans.*, 2012, **41**, 10014.
- 8 S. J. Li, S. X. Liu, C. C. Li, F. J. Ma, D. D. Liang, W. Zhang, R. K. Tan, Y. Y. Zhang and L. Xu, *Chem.-Eur. J.*, 2010, **16**, 13435.
- 9 L. S. Long, *CrystEngComm*, 2010, **12**, 1354.
- 10 (a) H. Y. Liu, H. Wu, J. Yang, Y. Y. Liu, B. Liu, Y. Y. Liu and J. F. Ma, *Cryst. Growth Des.*, 2011, **11**, 2920; (b) W. Q. Kan, J. F. Ma, Y. Y. Liu, H. Wu and J. Yang, *CrystEngComm*, 2011, **13**, 7037; (c) H. Wu, J. Yang, Y. Y. Liu and J. F. Ma, *Cryst. Growth Des.*, 2012, **12**, 2272.
- 11 (a) Y. Q. Lan, S. L. Li, X. L. Wang, K. Z. Shao, D. Y. Du, H. Y. Zang and Z. M. Su, *Inorg. Chem.*, 2008, **47**, 8179; (b) Y. Q. Lan, S. L. Li, X. L. Wang, K. Z. Shao, Z. M. Su and E. B. Wang, *Inorg. Chem.*, 2008, **47**, 529.
- 12 F. Yu, X. J. Kong, Y. Y. Zheng, Y. P. Ren, L. S. Long, R. B. Huang and L. S. Zheng, *Dalton Trans.*, 2009, 9503.
- 13 H. X. Yang, S. Y. Gao, J. Lü, B. Xu, J. X. Lin and R. Cao, *Inorg. Chem.*, 2010, **49**, 736.
- 14 J. Q. Sha, J. Peng, Y. Q. Lan, Z. M. Su, H. J. Pang, A. X. Tian, P. P. Zhang and M. Zhu, *Inorg. Chem.*, 2008, **47**, 5145.
- 15 (a) D. Drewes, E. M. Limanski and B. Krebs, *Eur. J. Inorg. Chem.*, 2004, **24**, 4849; (b) H. Y. An, D. R. Xiao, E. B. Wang, Y. G. Li and L. Xu, *New J. Chem.*, 2005, **29**, 667.
- 16 (a) V. Shivaiah, M. Nagaraju and S. K. Das, *Inorg. Chem.*, 2003, **42**, 6604; (b) A. M. Khenkin and R. Neumann, *Adv. Synth. Catal.*, 2002, **344**, 1017.
- 17 H. Y. An, X. Liu, H. Chen, Z. B. Han, H. Zhang and Z. F. Chen, *CrystEngComm*, 2011, **13**, 5384.
- 18 (a) P. P. Zhang, J. Peng, H. J. Pang, J. Q. Sha, M. Zhu, D. D. Wang, M. G. Liu and Z. M. Su, *Cryst. Growth Des.*, 2011, **11**, 2736; (b) X. Wang, J. Peng, K. Alimajea and Z. Y. Shi, *CrystEngComm*, 2012, **14**, 8509; (c) Z. Y. Shi, J. Peng, Y. G. Li, Z. Y. Zhang, X. Yu, K. Alimajea and X. Wang, *CrystEngComm*, 2013, **15**, 7583.
- 19 (a) X. Kuang, X. Wu, R. Yu, J. P. Donahue, J. Huang and C. Z. Lu, *Nat. Chem.*, 2010, **2**, 461; (b) Q. G. Zhai, X. Y. Wu, S. M. Chen, Z. G. Zhao and C. Z. Lu, *Inorg. Chem.*, 2007, **46**, 5046.
- 20 C. Streb, C. Ritchie, D. L. Long, P. KÓ§gerler and L. Cronin, *Angew. Chem., Int. Ed.*, 2007, **46**, 7579.
- 21 J. T. Rhule, W. A. Neiwert, K. I. Hardcastle, B. T. Do and C. L. Hill, *J. Am. Chem. Soc.*, 2001, **123**, 12101.
- 22 (a) H. Y. An, Y. G. Li, E. B. Wang, D. X. Xiao, C. Y. Sun and L. Xu, *Inorg. Chem.*, 2005, **44**, 6062; (b) H. Y. An, Y. G. Li, D. X. Xiao, E. B. Wang and C. Y. Sun, *Cryst. Growth Des.*, 2006, **6**, 1107.
- 23 (a) G. M. Sheldrick, *SHELXL 97, Program for Crystal Structure Refinement*, University of Göttingen, Germany, 1997; (b) G. M. Sheldrick, *SHELXL 97, Program for Crystal Structure Solution*, University of Göttingen, Germany, 1997.
- 24 (a) D. Sun, Z. H. Wei, C. F. Yang, D. F. Wang, N. Zhang, R. B. Huang and L. S. Zheng, *CrystEngComm*, 2011, **13**, 159; (b) M. Singh and A. Ramanan, *Cryst. Growth Des.*, 2011, **11**, 3381.
- 25 Q. Wu, W. L. Chen, D. Liu, C. Liang, Y. G. Li, S. W. Lin and E. B. Wang, *Dalton Trans.*, 2011, **40**, 56.
- 26 J. H. Yu and R. R. Xu, *Acc. Chem. Res.*, 2010, **43**, 1195.
- 27 G. K. Kole, G. K. Tan and J. J. Vittal, *Cryst. Growth Des.*, 2012, **12**, 326.
- 28 (a) G. B. Deacon and R. Phillips, *Coord. Chem. Rev.*, 1980, **33**, 227; (b) C. H. Li, K. L. Huang, Y. N. Chi, X. Liu, Z. G. Han, L. Shen and C. W. Hu, *Inorg. Chem.*, 2009, **48**, 2010.
- 29 I. D. Brown and D. Altermatt, *Acta Crystallogr., Sect. B: Struct. Sci.*, 1985, **41**, 244.
- 30 K. Saito, S. Kazama, K. Matsubara, T. Yui and M. Yagi, *Inorg. Chem.*, 2013, **52**, 8297.
- 31 (a) Y. Xia, P. F. Wu, Y. G. Wei, Y. Wang and H. Y. Guo, *Cryst. Growth Des.*, 2006, **6**, 253; (b) J. H. Liao, J. S. Juang and Y. C. Lai, *Cryst. Growth Des.*, 2006, **6**, 354.
- 32 (a) Y. G. Sun and Y. N. Xia, *Science*, 2002, **298**, 2176; (b) Y. N. Xia, Y. J. Xiong, B. K. Lim and S. E. Skrabalak, *Angew. Chem., Int. Ed.*, 2009, **48**, 60.
- 33 (a) S. Z. Du, X. M. Lu, J. Feng, Y. F. Cheng, L. An and X. J. Sun, *CrystEngComm*, 2012, **14**, 6618; (b) J. W. Wang and Y. D. Li, *Adv. Mater.*, 2003, **15**, 445.
- 34 W. J. Dong, Z. Shi, J. J. Ma, C. M. Hou, Q. Wan, S. H. Feng, A. Cogbill and Z. R. Tian, *J. Phys. Chem. B*, 2006, **110**, 5845.
- 35 (a) Y. F. Song, H. Abbas, C. Ritchie, N. McMillian, D. L. Long, N. Gadegaard and L. Cronin, *J. Mater. Chem.*, 2007, **17**, 1903; (b) T. McGlone, C. Streb, D. L. Long and L. Cronin, *Adv. Mater.*, 2010, **22**, 4275.
- 36 X. F. Kuang, X. Y. Wu, J. Zhang and C. Z. Lu, *Chem. Commun.*, 2011, **47**, 4150.